πNN coupling and two-pion photoproduction on the nucleon

Michihiro Hirata* and Nobuhiko Katagiri
Department of Physics, Hiroshima University, Higashi-Hiroshima 739, Japan

Takashi Takaki†
Department of Economics, Management and Information Science, Onomichi University, Onomichi 722-8506, Japan
(Received 22 October 2002; published 10 March 2003)

Effects of nonresonant photoproductions arising from two different πNN couplings are investigated in the $\gamma N \to \pi\pi N$ reaction. We find that the pseudoscalar (PS) πNN coupling is generally preferable to the pseudovector (PV) πNN coupling and particularly the total cross sections are successfully described by the model with the PS πNN coupling. In order to see the difference between the two couplings, we also show the results of invariant mass spectra and helicity-dependent cross sections in various isospin channels calculated with the PS and PV couplings.

DOI: 10.1103/PhysRevC.67.034601 PACS number(s): 25.20.Lj, 13.60.Rj, 25.20.Dc, 14.20.Gk

I. INTRODUCTION

Many experiments [1–9] of two-pion photoproductions on the nucleon have been performed in the past over the second nucleon-resonance energy, where the $N^*(1520)$ resonance plays an important role. Two charged pion photoproduction, i.e., $\gamma p \to \pi^+\pi^- p$, is well understood by theoretical models. However, none of the theoretical models have succeeded to explain the data of all isospin channels simultaneously. This means that there are some unknown production mechanisms that are not taken into account yet.

Recently, the total cross sections and invariant mass distributions of two-pion photoproductions followed by neutral pion emission, i.e., $\gamma p \to \pi^+\pi^0 n$ [6], $\gamma p \to \pi^0\pi^0 p$ [8], and $\gamma n \to \pi^-\pi^0 p$ [9] reactions, have been measured at the Mainz accelerator facility MAMI using the detector system with improved resolution at the photon energy up to around 0.8 GeV. The aim of these experiments was to obtain the information on the structure of the nucleon resonance and explore the reaction mechanisms. The $\gamma p \to \pi^+\pi^0 n$ and $\gamma n \to \pi^-\pi^0 p$ reactions have attracted special attention, since the detailed study of them could provide a new aspect on the reaction mechanisms, which are related to ρ meson production. There are notable differences between the $\pi^+\pi^0$ ($\pi^-\pi^0$) and $\pi^0\pi^0$ photoproductions. The ρ meson production as an intermediate process is allowed to the $\pi^+\pi^0$ ($\pi^-\pi^0$) photoproduction but is forbidden to the $\pi^0\pi^0$ photoproduction due to isospin conservation. On the other hand, the isospin $I=0$ $\pi\pi$ system such as σ meson may contribute to only the $\pi^0\pi^0$ photoproduction. Furthermore, the strength of the Δ Kroll-Rudermann process in the $\pi^+\pi^0(\pi^-\pi^0)$ photoproduction is weak compared with that in the $\pi^+\pi^-$ photoproduction, where its process dominates and is suppressed in the $\pi^0\pi^0$ photoproduction. Based on these characteristic features and the comparison between the measured $\pi^+\pi^0$ and $\pi^0\pi^0$ invariant mass distributions, Langgärtner *et al.* [6] concluded that the ρ decay of the $N^*(1520)$ resonance was directly observed in the $\gamma p \to \pi^+\pi^0 n$ reaction.

Theoretically, several works [10–14] have been already done to explain the total cross sections of two-pion photoproductions in various isospin channels. The total cross sections of the $\gamma p \to \pi^+\pi^- p$ reaction have been well reproduced by several theoretical models [10–14] where the Δ Kroll-Rudermann, Δ-pion-pole and $N^*(1520)$ resonant terms were found to be dominant. These models, however, could not predict the total cross sections of the above reactions accompanied by neutral pions consistently. The models of Tejedor-Oset [10] and Murphy-Laget [11] underestimated the cross sections of $\gamma p \to \pi^+\pi^0 n$ seriously, although the former model could reproduce the cross sections of $\gamma p \to \pi^0\pi^0 p$.

The model of Ochi, Hirata, and Takaki [12,13] could reproduce the $\gamma p \to \pi^+\pi^0 n$ and $\gamma n \to \pi^-\pi^0 p$ cross sections as well as $\gamma p \to \pi^+\pi^- p$ cross sections, although it underestimated the $\gamma p \to \pi^0\pi^0 p$ cross sections. Their calculations indicated that the ρ meson productions, i.e., the $N^*(1520) \to \rho N$ process and ρ Kroll-Ruderman process, play an essential role in the $\gamma p \to \pi^+\pi^0 n$ and $\gamma n \to \pi^-\pi^0 p$ reactions where the mass of ρ meson produced in the intermediate state is always smaller than the on-shell value at the relevant energies. In their model, the ρ meson is treated in a dynamical way where the finite-range $\rho\pi\pi$ form factor is assumed. In order to obtain large cross sections of the $\gamma p \to \pi^+\pi^0 n$ and $\gamma n \to \pi^-\pi^0 p$ reactions, a rather soft $\rho\pi\pi$ form factor, which makes the contribution of the ρ Kroll-Ruderman term large, was needed. Because of the soft $\rho\pi\pi$ form factor, however, the dynamical model for the ρ meson overestimates the $\pi\pi$ p-wave (isospin $I=1$) phase shifts at low energies. They speculated that the large ρ Kroll-Ruderman term in their model might simulate a background process in the isospin $I=1$ channel effectively rather than the ρ meson production. The presence of such a background process is inferred from the fact that in the isovector $\pi\pi$ spectral function derived from the $\pi\pi \to N\bar{N}$ helicity amplitudes [15], there is a strong enhancement near the $\pi\pi$ threshold as well

*Email address: hirata@theo.phys.sci.hiroshima-u.ac.jp
†Email address: takaki@onomichi-u.ac.jp

as the resonant structure by the ρ meson. This bump at low energies is actually due to the nonresonant process described by the partial amplitude of the nucleon Born term projected to the $I=J=1$ $\pi\pi(N\bar{N})$ channel.

In this paper, motivated by the above speculation, we will investigate the effect of the nonresonant reaction mechanisms, particularly, the background terms arising from the πNN coupling that were so far considered to have only small contributions to the cross sections and were always taken to be the pseudovector (PV) coupling. In the studies of single-pion photoproductions, it has been shown that the PV πNN coupling is preferred at low energies but the pseudoscalar (PS) πNN coupling is needed to get a better description at higher energies [16] and furthermore the two πNN couplings lead to rather different cross sections for the neutral pion production [17]. These facts imply that the PS coupling becomes important at larger off-shell nucleon momenta and thus will have a significant influence on the two-pion photoproductions accompanied by the neutral pion such as the $\gamma p\to\pi^+\pi^0 n$ and $\gamma p\to\pi^0\pi^0 p$ reactions. In our calculations with two different couplings, we will show that the nonresonant photoproduction by the PS coupling significantly contributes to the total cross sections of the two-pion photoproductions involving the neutral pion compared with that by the PV coupling and consequently plays a similar role with the strong ρ Kroll-Ruderman term introduced in the model by Ochi and co-workers [12,13]. From the comparison between the full calculations with resonant processes and the experimental data, furthermore, we will demonstrate that the PS coupling is more favored than the PV coupling for the two-pion photoproductions at the relevant energies.

Recently, Nacher *et al.* [14] have improved the model of Tejedor and Oset [10] by including the $\Delta(1700)$ production and the ρ meson effect arising from the $N^*(1520)$ production. In their calculations with the PV coupling, they found that the ρ meson effect largely increased the $\gamma p\to\pi^+\pi^0 n$ total cross sections compared with the previous model and put the calculations close to the data, although there still remained some disagreement with the data around the peak for both the $\gamma p\to\pi^+\pi^0 n$ and $\gamma p\to\pi^0\pi^0 p$ cross sections. We will discuss why their model can largely improve the calculations of the $\gamma p\to\pi^+\pi^0 n$ cross sections without introducing the strong ρ Kroll-Ruderman term used in the model by Ochi and co-workers [12,13].

In Sec. II, we will discuss the background processes and πNN coupling. In Sec. III, we will review how to treat the resonance processes. In Sec. IV, we will show our full calculations of the total cross sections, invariant mass spectra and helicity-dependent cross sections and discuss the difference between the PS and PV couplings from the comparison with the data. In Sec. V, we will give our concluding remarks.

II. NONRESONANT PROCESSES AND πNN COUPLING

In this section we discuss the nonresonant processes arising from the πNN coupling and vector mesons. There are two types of πNN couplings: the PS coupling and the PV coupling. The Lagrangian is

$$\mathcal{L}^{PS}_{\pi NN}=ig_{\pi NN}\bar{\psi}\gamma^5\boldsymbol{\tau}\psi\boldsymbol{\phi} \tag{1}$$

for the PS coupling, and

$$\mathcal{L}^{PV}_{\pi NN}=\frac{f_{\pi NN}}{m_\pi}\bar{\psi}\gamma^\mu\gamma^5\boldsymbol{\tau}\psi\partial_\mu\boldsymbol{\phi} \tag{2}$$

for the PV coupling, where ψ and $\boldsymbol{\phi}$ are the nucleon and pion fields, respectively, $g^2_{\pi NN}/4\pi=14.4$ and $f_{\pi NN}/m_\pi=-g_{\pi NN}/2M_N$ and m_π and M_N are the pion and nucleon masses, respectively. These couplings are equivalent when both the nucleons are on shell. If a photon line is attached to the πNN system so as to become gauge-invariant, one obtains the Feynman diagrams of the Born terms for the one-pion photoproduction whose expressions depend on the πNN coupling. The π Kroll-Ruderman term is included in the PV Born terms. The Born terms calculated with the two couplings are rather different from each other because of their different off-shellness. The PV coupling is preferable to the PS coupling at low energies because the PV Born terms are consistent with low energy theorems and current algebra predictions. In fact, the model with the PV coupling is able to reproduce the E_{0+} multipole up to the $\Delta(1232)$ resonance energy region but the model with the PS coupling fails. As the incident photon energy increases over 500 MeV, however, the pure PV coupling cannot explain the E_{0+} and M_{1-} multipoles and the PS coupling is needed to describe them [16]. This suggests that the πNN vertex for the far off-shell nucleon is largely pseudoscalar in nature. We note that only the multipoles E_{0+} and M_{1-} are affected by changing the coupling scheme and the two πNN couplings give rise to significantly different cross sections for the neutral pion photoproduction but are almost indistinguishable in the charged pion photoproduction. Therefore, it is interesting to see the difference between the PV and PS couplings in the two-pion photoproduction around the $N^*(1520)$ resonance energy region, where the far off-shell nucleons are involved in the intermediate state.

Before going to the $\gamma N\to\pi\pi N$ reaction, we discuss briefly the strong interaction part relevant to the two-pion production. In the $\pi N\to\pi N$ scattering at low energies, the Born terms constructed with the PV coupling are also preferable to those with the PS coupling like the $\gamma N\to\pi N$ reaction. In this case, for instance, the *s*-wave isoscalar scattering length calculated from the PS Born terms is very large and in disagreement with the data. In dispersion relation theory, the PS Born terms correspond to nucleon-pole terms and the PV Born terms are understood to include strong corrections coming from the dispersive integral in addition to the pole terms. These corrections are important to well describe the low energy data of the πN scattering and may be partially related to the σ meson exchange contribution as inferred from the linear σ model. When constructing the model for the $\gamma N\to\pi\pi N$ reaction with the PS πNN coupling, these corrections must be taken into account. To do so, we introduce the following effective Lagrangian:

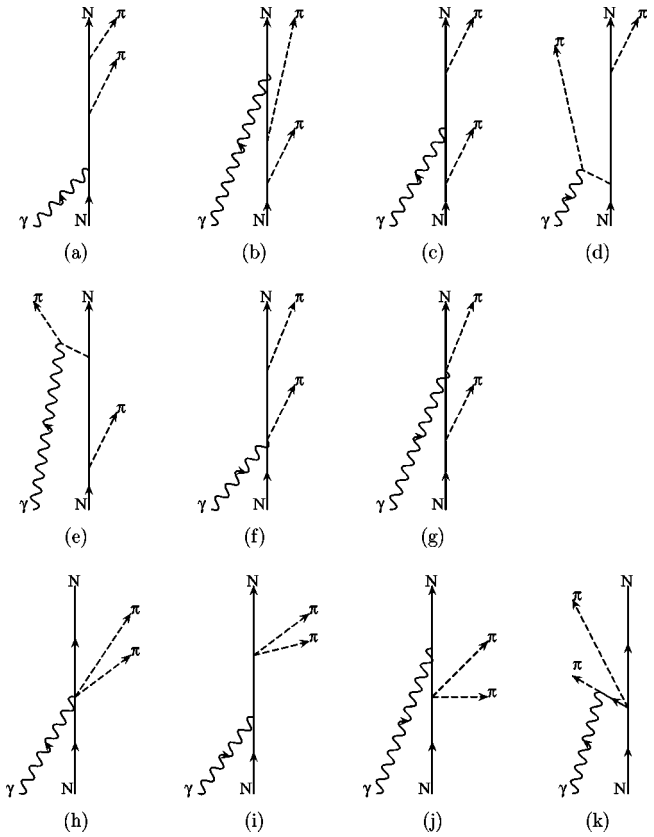

FIG. 1. Diagrams of Born terms arising from πNN coupling (a)–(g) and the effective Lagrangian of Eq. (3) (h)–(k).

$$\mathcal{L}_{\pi\pi NN}=\frac{g^2_{\pi NN}}{2M_N}\bar{\psi}\psi\boldsymbol{\phi}\cdot\boldsymbol{\phi}+\frac{g^2_{\pi NN}}{(2M_N)^2}\bar{\psi}\gamma^\mu\boldsymbol{\tau}\psi(\boldsymbol{\phi}\times\partial_\mu\boldsymbol{\phi}). \quad (3)$$

The sum of the PS Born terms and their correction terms calculated from the above effective Lagrangian are equivalent to the PV Born terms for the strong interaction processes such as $\pi N\to\pi N$ and $N\to\pi\pi N$. We note that the πN isoscalar scattering length calculated in these models are consistent with the value obtained by taking $m_\sigma\to\infty$ in the linear σ model, where m_σ is the σ meson mass.

The diagrams shown in Fig. 1 for the $\gamma N\to\pi\pi N$ reaction are obtained by attaching an external photon line to the diagrams of the $N\to\pi\pi N$ processes based on the requirement of the gauge invariance. The diagrams calculated with the PV coupling correspond to Figs. 1(a)–1(g) and especially the diagrams (f) and (g) include the π Kroll-Rutherman term arising from the derivative πNN coupling. On the other hand, the diagrams calculated with the PS coupling and the above effective Lagrangian correspond to Figs. 1(a)–1(e) and 1(h)–1(k), respectively. They will be referred to as PV model and PS model, respectively. For the second term (isovector term) of Eq. (3), only the diagram (k) of Fig. 1 is computed in actual calculations because the contributions of the other diagrams are negligible. Here the Lagrangians for the γNN and $\gamma\pi\pi$ couplings are given by

$$\mathcal{L}_{\gamma NN}=-e\bar{\psi}[F_1\gamma^\mu A_\mu-F_2\sigma^{\mu\nu}(\partial_\nu A_\mu)]\psi, \quad (4)$$

$$\mathcal{L}_{\gamma\pi\pi}=e(\partial_\mu\boldsymbol{\phi}\times\boldsymbol{\phi})_3A^\mu, \quad (5)$$

where A_μ is the photon field, and F_1 and F_2 are the electromagnetic form factors, which are taken to be $F_1=1$ and $F_2=1.79/(2M_N)$ for the proton and $F_1=0$ and $F_2=-1.91/(2M_N)$ for the neutron, respectively. The other Lagrangians for coupling of a photon and hadrons are obtained from the minimal substitution ($\partial_\mu\to\partial_\mu+ieA_\mu$) in the Lagrangians of πNN and $\pi\pi NN$ derivative vertices. The resultant amplitudes for the $\gamma N\to\pi\pi N$ reaction will give rather different cross sections depending on whether the PS model or PV model is used because of their different off-shell behavior, as expected from the above discussion about the $\gamma N\to\pi N$ reaction. We will show the difference from the numerical results later. As other nonresonant processes, we include the contributions of vector mesons such as ρ meson and ω meson. In the analysis of the $\gamma N\to\pi N$ reaction, these contributions are known to be important although their magnitude is small. The hadronic Lagrangians involving these vector mesons are

$$\mathcal{L}_{\rho NN}=-\bar{\psi}\left(g^V_{\rho NN}\gamma^\mu-\frac{g^T_{\rho NN}}{2M_N}\sigma^{\mu\nu}\partial_\nu\right)\boldsymbol{\rho}_\mu\cdot\boldsymbol{\tau}\psi, \quad (6)$$

$$\mathcal{L}_{\rho\pi\pi}=-f_\rho\boldsymbol{\rho}_\mu\cdot(\boldsymbol{\phi}\times\partial^\mu\boldsymbol{\phi}), \quad (7)$$

$$\mathcal{L}_{\omega NN}=-\bar{\psi}\left(g^V_{\omega NN}\ \gamma^\mu-\frac{g^T_{\omega NN}}{2M_N}\sigma^{\mu\nu}\partial_\nu\right)\omega_\mu\psi, \quad (8)$$

where $\boldsymbol{\rho}_\mu$ and ω_μ are the ρ and ω meson fields, respectively, and the coupling constants are taken to be $g^V_{\rho NN}=2.9, g^T_{\rho NN}=18.15, f_\rho=6.0, g^V_{\omega NN}=7.98$, and $g^T_{\omega NN}=0$. The electromagnetic Lagrangian for the $\gamma\pi_0\omega$ coupling is

$$\mathcal{L}_{\gamma\pi_0\omega}=-\frac{g_{\gamma\pi\omega}}{m_\omega}\varepsilon_{\mu\nu\rho\sigma}(\partial^\mu A^\nu)\pi_0\partial^\rho(\omega^\sigma), \quad (9)$$

where $g_{\gamma\pi\omega}=0.374e$ and $m_\omega=783$ MeV. The other electromagnetic Lagrangians are derived from the minimal substitution as done for the PS and PV models before. The diagrams for the $\gamma N\to\pi\pi N$ reaction involving the ρ and ω mesons are shown in Fig. 2 and are calculated by using the above Lagrangians. For the ω meson contribution, diagrams (g) and (h) in Fig. 2 are taken into account. The diagram (c) (called ρ Kroll-Ruderman term) comes from the derivative ρNN tensor coupling. In the diagrams of (a)–(d) in Fig. 2, the ρ meson decays into two real pions directly and so the ρ propagator D_ρ must include the decay effect, whose form is assumed to be

$$D_\rho(\sqrt{s})=\frac{1}{s-m_\rho^2+im_\rho\Gamma_\rho(\sqrt{s})}, \quad (10)$$

with

$$\Gamma_\rho(\sqrt{s})=\frac{2}{3}\frac{f_\rho^2}{4\pi s}\mathbf{q}^3_{cm.} \quad (11)$$

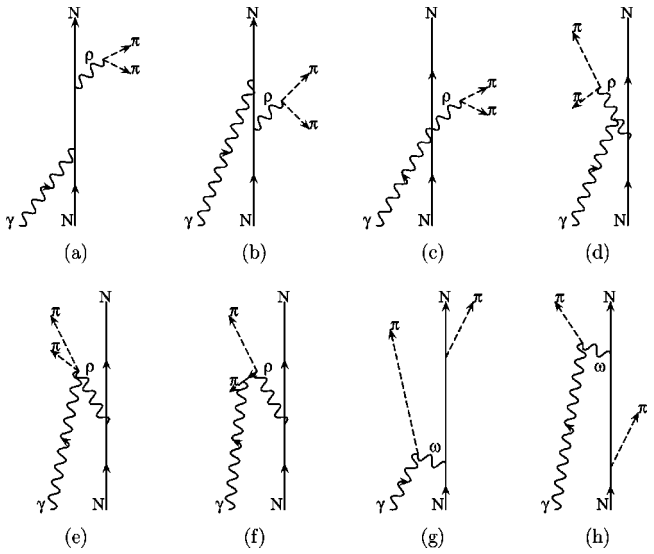

FIG. 2. Diagrams of nonresonant processes arising from ρ and ω mesons.

Here the ρ meson mass $m_\rho = 775$ MeV, its width $\Gamma_\rho(m_\rho) = 150$ MeV, and $\mathbf{q}_{cm}$ stands for the pion momentum in the $\pi\pi$ center-of-mass system. In our present model, the ρ meson displayed in Fig. 2 is treated in the same way used in Refs. [10,14] where the $\rho\pi\pi$ vertex function is simply given by the Lagrangian of Eq. (7). Even though one uses the $\rho\pi\pi$ vertex function with the finite-range form factor employed in Refs. [12,13], there is no drastic numerical change from the above way in the magnitude of the ρ Kroll-Ruderman term as far as one uses the range parameter determined so as to reproduce the $\pi\pi$ p-wave (isospin $I=1$) phase shifts.

For the diagrams involving the off-shell meson coupled to nucleon in Figs. 1 and 2, we take into account a form factor of the following form:

$$F(q^2) = \frac{\Lambda^2 - m^2}{\Lambda^2 - q^2}, \tag{12}$$

where m and q^2 are the meson mass and the square of four momentum, respectively and the range parameter Λ is taken to be $\Lambda = 1.25$ GeV for π, $\Lambda = 1.4$ GeV for both ρ and ω, respectively [14]. The pion form factor is used for the diagrams (d) and (e) in Fig. 1 and the ρ meson and ω meson form factors are used for (a)–(f) and (g)–(h) in Fig. 2, respectively. For the diagrams (f) and (g) in Fig. 1 (π Kroll-Ruderman term), the same pion form factor is used and evaluated at the momentum transfer between the incident photon and the outgoing pion. The diagram (c) in Fig. 2 (ρ Kroll-Ruderman term) is treated in the same way as the π Kroll-Ruderman term. We note that the gauge invariance of the transition amplitudes is destroyed by the inclusion of the decay width in the propagator and the form factor for the hadronic vertex. However, we consider such strong interaction corrections are more important than the gauge invariance from a phenomenological point of view. In fact, the form factor used in the Δ Kroll-Ruderman term [see Fig. 5(a)] influences significantly on the magnitude of the $\gamma p \to \pi^+\pi^- p$ cross section and provides a good agreement with the data [10].

Now we discuss the differences between the PS and PV models through numerical calculations of the cross sections. The cross section for the $\gamma N \to \pi_\alpha \pi_\beta N$ reaction is given by

$$\sigma = \frac{1}{2|\mathbf{k}|}\frac{M_N}{E_{p_1}}\frac{1}{v_{rel}}\int \frac{d^3p_2}{(2\pi)^3}\frac{d^3q_\alpha}{(2\pi)^3}\frac{d^3q_\beta}{(2\pi)^3}\frac{M_N}{E_{p_2}}\frac{1}{2\omega_\alpha}\frac{1}{2\omega_\beta} \times (2\pi)^4\delta^{(4)}(p_1 + k - p_2 - q_\alpha - q_\beta) \times \sum_{\nu\nu'}\frac{1}{2}|\langle 1/2,\nu'|T|1/2,\nu\rangle|^2, \tag{13}$$

where $k = (|\mathbf{k}|,\mathbf{k})$, $p_1 = (E_{p_1},\mathbf{p}_1)$, $p_2 = (E_{p_2},\mathbf{p}_2)$, and $q_\gamma = (\omega_\gamma,\mathbf{q}_\gamma)$ ($\gamma = \alpha,\beta$) are the four-momenta of the initial photon, initial nucleon, final nucleon, and outgoing pion, respectively, v_{rel} is the relative velocity between the initial nucleon and photon, and $\omega_\gamma = \sqrt{m_\pi^2 + \mathbf{q}_\gamma^2}$ and $E_p = \sqrt{M_N^2 + p^2}$. The cross section is evaluated in the γN center-of-mass system. The T matrix is in general expressed as $T = A + i\boldsymbol{\sigma}\cdot\mathbf{B}$, which is summed over the final nucleon spin states (ν') and averaged over the initial nucleon spin states (ν).

We show how to evaluate the T matrix by taking one of the diagrams as an example. Let us consider the process corresponding to (a) in Fig. 1 computed with the PS coupling. The T matrix is divided into two parts of the hadronic process and electromagnetic process and then into the particle and anti-particle intermediate states for the convenience. Thus, the T matrix is expressed as

$$\chi^\dagger T\chi = H^{(1)}_{\gamma NN}\frac{1}{E_{p_2} - k - E_{p_2-k}}\frac{M_N}{E_{p_2-k}}H^{(1)}_{NN\pi\pi} + H^{(2)}_{\gamma NN}\frac{1}{E_{p_2} - k + E_{p_2-k}}\frac{M_N}{E_{p_2-k}}H^{(2)}_{NN\pi\pi}, \tag{14}$$

where the transition matrices H are given by

$$H^{(1)}_{\gamma NN} = e\overline{u}(\mathbf{p}_2)(F_1\boldsymbol{\gamma}\cdot\boldsymbol{\varepsilon} - iF_2\sigma^{i\nu}\varepsilon_i k_\nu)u(\mathbf{p}_2 - \mathbf{k}) \simeq \chi^\dagger e(S_E^{(1)} + i\boldsymbol{\sigma}\cdot\mathbf{V}_E^{(1)})\chi, \tag{15}$$

with

$$S_E^{(1)} = \sqrt{\frac{E_{p_2} + M_N}{2M_N}}\sqrt{\frac{E_{p_2-k} + M_N}{2M_N}} \times \left(\frac{F_1 + F_2 k}{E_{p_2-k} + M_N} + \frac{F_1 - F_2 k}{E_{p_2} + M_N}\right)\mathbf{p}_2\cdot\boldsymbol{\varepsilon}, \tag{16}$$

$$\mathbf{V}_E^{(1)} = \sqrt{\frac{E_{p_2}+M_N}{2M_N}}\sqrt{\frac{E_{p_2-k}+M_N}{2M_N}} \times\left[\frac{F_1+(E_{p_2-k}+M_N+k)F_2}{E_{p_2-k}+M_N}\mathbf{k}\times\boldsymbol{\varepsilon} -\left(\frac{F_1+F_2k}{E_{p_2-k}+M_N}+\frac{F_1-F_2k}{E_{p_2}+M_N}\right)\mathbf{p}_2\times\boldsymbol{\varepsilon}\right], \quad (17)$$

for the $\gamma N\rightarrow N$ process,

$$H_{NN\pi\pi}^{(1)} = \overline{u}(\mathbf{p}_2-\mathbf{k})g_{\pi NN}\gamma^5\tau_\beta\frac{\not p_1-\not q_\alpha+M_N}{(p_1-q_\alpha)^2-M_N^2} \times g_{\pi NN}\gamma^5\tau_\alpha u(\mathbf{p}_1) \simeq \chi^\dagger g_{\pi NN}^2(S_1^{(1)}+i\boldsymbol{\sigma}\cdot\mathbf{V}_1^{(1)})\chi, \quad (18)$$

with

$$S_1^{(1)} = \sqrt{\frac{E_{p_2-k}+M_N}{2M_N}}\sqrt{\frac{E_{p_1}+M_N}{2M_N}} \times\left[\omega_\alpha-\left(\frac{\mathbf{q}_\alpha\cdot\mathbf{p}_1}{E_{p_1}+M_N}+\frac{\mathbf{q}_\alpha\cdot(\mathbf{p}_1-\mathbf{k})}{E_{p_1-k}+M_N}\right)\right] \times\frac{\tau_\beta\tau_\alpha}{(p_1-q_\alpha)^2-M_N^2}, \quad (19)$$

$$\mathbf{V}_1^{(1)} = \sqrt{\frac{E_{p_2-k}+M_N}{2M_N}}\sqrt{\frac{E_{p_1}+M_N}{2M_N}} \times\left[\left(\frac{1}{E_{p_2-k}+M}-\frac{1}{E_{p_1}+M}\right)(\mathbf{q}_\alpha\times\mathbf{p}_1) -\frac{\mathbf{q}_\alpha\times\mathbf{q}_\beta}{E_{p_2-k}+M_N}\right]\frac{\tau_\beta\tau_\alpha}{(p_1-q_\alpha)^2-M_N^2} \quad (20)$$

for the $N\rightarrow\pi\pi N$ process,

$$H_{\gamma NN}^{(2)} = \overline{u}(\mathbf{p}_2)e(F_1\boldsymbol{\gamma}\cdot\boldsymbol{\varepsilon}-iF_2\sigma^{i\nu}\varepsilon_i k_\nu)v(-\mathbf{p}_2+\mathbf{k}) \simeq \chi^\dagger e(-i)(S_E^{(2)}+i\boldsymbol{\sigma}\cdot\mathbf{V}_E^{(2)})\chi, \quad (21)$$

with

$$S_E^{(2)} = \sqrt{\frac{E_{p_2}+M_N}{2M_N}}\sqrt{\frac{E_{p_2-k}+M_N}{2M_N}} \times\left(\frac{F_2}{E_{p_2-k}+M_N}+\frac{F_2}{E_{p_2}+M_N}\right)(\mathbf{k}\times\boldsymbol{\varepsilon})\cdot\mathbf{p}_2, \quad (22)$$

$$\mathbf{V}_E^{(2)} = \sqrt{\frac{E_{p_2}+M_N}{2M_N}}\sqrt{\frac{E_{p_2-k}+M}{N}}2M_N \times\left[\left\{F_1+\left(k-\frac{k^2}{E_{p_2-k}+M_N}\right)F_2\right\}\boldsymbol{\varepsilon} +F_2\left(\frac{1}{E_{p_2-k}+M_N}-\frac{1}{E_{p_2}+M_N}\right)(\mathbf{k}\times\boldsymbol{\varepsilon})\times\mathbf{p}_2\right], \quad (23)$$

for the $\gamma\rightarrow N\overline{N}$ process and

$$H_{N\overline{N}\pi\pi}^{(2)} = \overline{v}(-\mathbf{p}_2+\mathbf{k})g_{\pi NN}\gamma^5\tau_\beta i\frac{\not p_1-\not q_\alpha+M}{(p_1-q_\alpha)^2-M^2} \times g_{\pi NN}\gamma^5\tau_\alpha u(\mathbf{p}_1) \simeq \chi^\dagger g_{\pi NN}^2(-i)(S_1^{(2)}+i\boldsymbol{\sigma}\cdot\mathbf{V}_1^{(2)})\chi \quad (24)$$

with

$$S_1^{(2)} = 0, \quad (25)$$

$$\mathbf{V}_1^{(2)} = -\sqrt{\frac{E_{p_2-k}+M_N}{2M_N}}\sqrt{\frac{E_{p_1}+M_N}{2M_N}} \times\left[\mathbf{q}_\alpha+\left(\frac{1}{E_{p_2-k}+M_N}-\frac{1}{E_{p_1}+M_N}\right)\omega_\alpha\mathbf{p}_1 -\frac{\omega_\alpha(\mathbf{q}_\alpha+\mathbf{q}_\beta)}{E_{p_2-k}+M_N}\right]\frac{\tau_\beta\tau_\alpha}{(p_1-q_\alpha)^2-M_N^2} \quad (26)$$

for the $N\overline{N}\rightarrow\pi\pi$ process, respectively. Here u and v are the Dirac spinors for nucleon and antinucleon, respectively and χ is the two-component spinor. In this expression, we neglect the $O[(E_p+M_N)^{-2}]$ contributions. However, we found this approximate T matrix gives nearly the same result as the exact one within the present energy region. The calculations for the other diagrams are performed in a similar fashion. In this sense, the T matrix is evaluated in a relativistic way.

In order to estimate the relativistic effect, we calculated the cross section with the PV coupling for the diagrams (a)–(g) in Fig. 1 in both relativistic and nonrelativistic ways. Here nonrelativistic approximations mean that both the antiparticle contributions and terms of order $(p/M_N)^2$ or higher in vertex operators are neglected but the denominators of the propagator are treated in a relativistic way. We found that the relativistic calculations are about 30–60 % larger than the nonrelativistic calculations around the $N^*(1520)$ resonance energy. This indicates that the relativistic effect, which have been so far neglected in previous studies, should not be discarded for the nonresonant process in the $\gamma N\rightarrow\pi\pi N$ reaction.

Now we show the calculations of total cross sections for three isospin channels: $\gamma p\rightarrow\pi^+\pi^- p$, $\gamma p\rightarrow\pi^+\pi^0 n$, and $\gamma p\rightarrow\pi^0\pi^0 p$ in Fig. 3. Here solid and dashed lines correspond to the full nonresonant calculations for the PS and PV

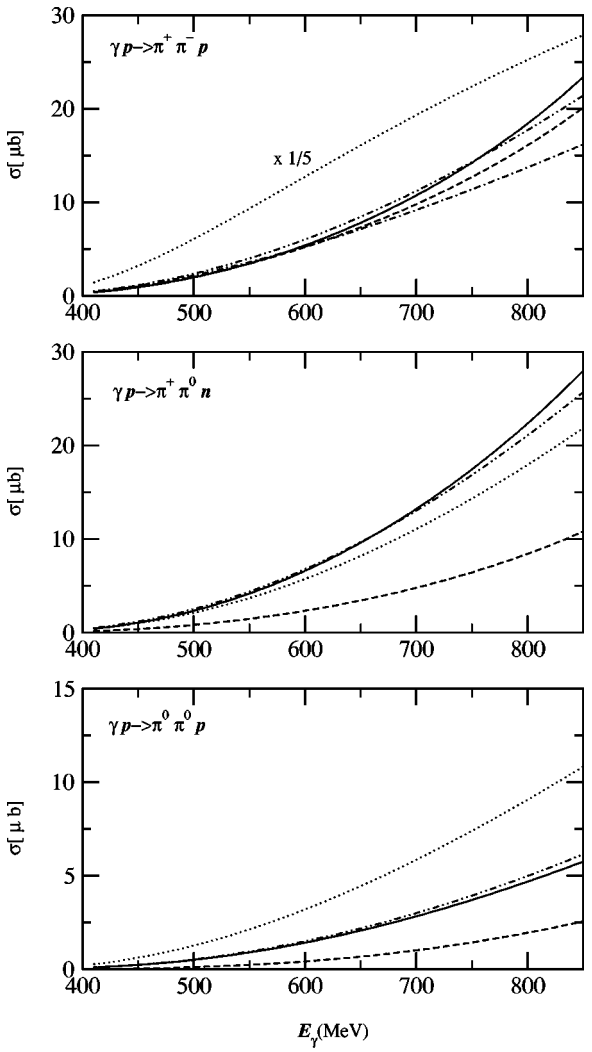

FIG. 3. Nonresonant contributions to total cross sections for $\gamma p \to \pi^+ \pi^- p$, $\gamma p \to \pi^+ \pi^0 n$, and $\gamma p \to \pi^0 \pi^0 p$ reactions. The solid and dashed lines correspond to the PS and PV calculations with the vector meson contributions, respectively. The meaning of remaining lines is given in the text.

models including the vector meson contributions (Fig. 2), respectively. We observe that the PV results of the $\pi^+ \pi^-$ channel are close to the PS results, while in the $\pi^+ \pi^0$ and $\pi^0 \pi^0$ channels there are significant differences and the PS calculations are larger than the PV calculations. The similar feature can be seen in the one-pion photoproduction where the difference between two couplings is prominent in the neutral pion photoproduction but is very small in the charged pion photoproduction. This arises certainly from the different off-shell behavior between the PV and PS πNN couplings. For the one-pion photoproduction, such difference appears in the Born terms proportional to the anomalous magnetic moment obtained using the second term of Eq. (4). In fact, if F_2 is set to zero, the difference between the PS and PV calculations disappears. The same things happen for the two-pion photoproduction, which has been examined numerically.

It is interesting to observe that the PS calculation in the $\gamma p \to \pi^+ \pi^0 n$ channel is remarkably larger than the PV calculation and is roughly consistent with the size of the ρ Kroll-Ruderman term introduced in the model of Ochi *et al.* [12,13], by which the large measured cross sections have been successfully explained. In order to reproduce the data, however, the small range paramater of the $\rho \pi \pi$ form factor must have been used and it gave rise to the larger $\pi \pi$ scattering p-wave phase shift at low energies compared with the experimental value. We think that the ρ Kroll-Ruderman term with this form factor simulates a non-negligible background process originating from the strong coupling between the nucleon and $I=J=1$ $\pi \pi$ system as is inferred from strong enhancement at low energies in the isovector $\pi \pi$ spectral function derived from the $\pi \pi \to N \bar{N}$ helicity amplitude [15]. Therefore, the ρ Kroll-Ruderman term is considered to represent the nonresonant process arising from the PS coupling effectively.

In Fig. 3, we also show the results for the Born terms coming from the PS coupling (dotted lines) corresponding to the diagrams (a)–(e) in Fig. 1. We find that the contribution to the $\gamma p \to \pi^+ \pi^- p$ channel is extremely large and is mostly attributed to the pion-pole terms [diagrams (d) and (e) in Fig. 1]. The similar situation occurs when one calculates the πN isoscalar s-wave scattering length with the PS coupling. These unfavorable results can be improved by introducing the contact interaction of Eq. (3) as mentioned before. This effect is seen in the calculations with the contact terms (dash-two-dotted lines in Fig. 3). Here the contact terms correspond to the diagrams (h)–(k) in Fig. 1 and consist of the isoscalar and isovector parts. The isoscalar term contributes to the $\gamma p \to \pi^+ \pi^- p$ and $\gamma p \to \pi^0 \pi^0 n$ channels and the isovector term contributes to the $\gamma p \to \pi^+ \pi^- p$ and $\gamma p \to \pi^+ \pi^0 n$ channels, and the isoscalar term has larger coupling constant than the isovector term as understood from Eq. (3). The size of these terms can be seen in the calculations in Fig. 3.

For comparison, the result for the Born terms coming from the PV coupling [diagrams (a)–(g) in Fig. 1] is also shown by dash-dotted line in Fig. 3. The dash-dotted line is drawn only in the $\gamma p \to \pi^+ \pi^- p$ channel but omitted in other channels since the full nonresonant calculations (dashed line) in other channels are almost overlapped with the dash-dotted line. The difference between the solid and dash-two-dotted lines or between the dashed and dash-dotted lines arises from the vector meson contributions of the diagrams in Fig. 2. The contributions are relatively small. This smallness is mainly attributed to the effect of form factors used. In this paper, we do not pursue this effect furthermore.

In order to see the difference between the PS and PV models in further detail, the $\pi \pi$ invariant-mass spectra are calculated and the results at 750 MeV are shown in Fig. 4. The meaning of lines is the same as that of Fig. 3. Apart from the size of the distributions, the difference of the shape can be seen in these distributions, especially in the $\gamma p \to \pi^0 \pi^0 p$ channel. Even in the PS calculations for the $\gamma p \to \pi^+ \pi^- p$ and $\gamma p \to \pi^+ \pi^0 n$ channels, there are some shifts of the peak to the higher invariant mass compared with the PV calculations. Here it is interesting to note that the $I=J=1$ $\pi \pi$ system relevant to the ρ meson can contribute to the

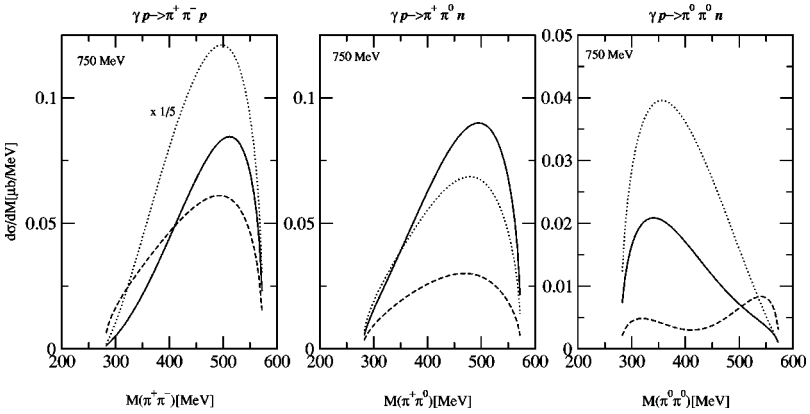

FIG. 4. Nonresonant contributions to the $\pi\pi$ invariant mass spectra for $\gamma p \to \pi^+\pi^- p$, $\gamma p \to \pi^+\pi^0 n$, and $\gamma p \to \pi^0\pi^0 p$ reactions at 750 MeV. The meaning of lines is the same as that of Fig. 3.

$\gamma p \to \pi^+\pi^- p$ and $\gamma p \to \pi^+\pi^0 n$ reactions and on the other hand the $I=J=0$ $\pi\pi$ system relevant to the σ meson can contribute to the $\gamma p \to \pi^+\pi^- p$ and $\gamma p \to \pi^0\pi^0 p$ reactions. The correlations for the final $\pi\pi$ system might influence both the shape and size of the distributions but in our calculations they are not taken into account. In this work, as a first step, we would like to demonstrate how different the PS and PV models are within our present framework. In order to compare the calculations with the experimental data, the resonant contributions must be included. We will employ a simple model for the resonant processes, which will be discussed in the following section.

III. RESONANT PROCESSES

A. Isobar model

The two-pion photoproduction in the second resonance energy region involves the resonances such as ρ meson, $\Delta(1232)$ and $N^*(1520)$ as important intermediate states. We treat these resonances with the isobar model, where the scattering of $\pi\pi$ or πN in the relevant channel is assumed to be described solely by the resonant state. We employ the same formalism used in Refs. [12,13], which is briefly reviewed in this section.

In this model, the $\pi\pi$ p-wave scattering t matrix in the energies from threshold to the ρ meson resonance is assumed to be written as

$$t_{\pi\pi} = \frac{F_{\rho\pi\pi} F^{\dagger}_{\rho\pi\pi}}{2m^0_\rho(\sqrt{s} - m^0_\rho - \Sigma_{\rho\pi\pi})}, \tag{27}$$

where m^0_ρ and $\sqrt{s}$ denote the bare mass of ρ meson and the $\pi\pi$ center-of-mass energy, respectively. The $\rho\pi\pi$ vertex function is assumed to have the form

$$F_{\rho\pi\pi} = 2h_\rho(\kappa)(\boldsymbol{\varepsilon}_\rho \cdot \boldsymbol{\kappa}),$$
$$h_\rho(\kappa) = \frac{f_{\rho\pi\pi}}{1 + (\kappa/q_{\rho\pi\pi})^2}, \tag{28}$$

where $f_{\rho\pi\pi}$ and $q_{\rho\pi\pi}$ are the $\rho\pi\pi$ coupling constant and range parameter, respectively, and $\boldsymbol{\varepsilon}_\rho$ is the polarization vector and $\boldsymbol{\kappa}$ is the relative momentum between two pions. The ρ self-energy $\Sigma_{\rho\pi\pi}$ is evaluated with the same way used in Ref. [12]. The parameters m^0_ρ, $f_{\rho\pi\pi}$, and $q_{\rho\pi\pi}$ are determined to fit the $\pi\pi$ p-wave phase shifts as well as the mass and width of ρ meson. We take $m^0_\rho = 910$ MeV, $f_{\rho\pi\pi} = 7.8$, and $q_{\rho\pi\pi} = 800$ MeV/c, which are used in the calculation of the N^* self-energy. In the previous paper [12,13], $q_{\rho\pi\pi}$ was adjusted to fit the $\gamma p \to \pi^+\pi^0 n$ data instead of the $\pi\pi$ p-wave phase shifts. In the case of Ref. [13], $q_{\rho\pi\pi}$ was taken to be 200 MeV/c, which made the size of the ρ Kroll-Ruderman term quite large. This parametrization was only a way to phenomenologically reproduce the $\gamma p \to \pi^+\pi^0 n$ reaction cross section within the previous model.

The πN scattering t matrix in the P_{33} channel is written as

$$t_{P33} = \frac{F_{\pi N\Delta} F^{\dagger}_{\pi N\Delta}}{\sqrt{s} - M^0_\Delta - \Sigma^\Delta_{\pi N}}, \tag{29}$$

where $\sqrt{s}$ and M^0_Δ denote the πN center-of-mass energy and bare mass of $\Delta(1232)$, respectively. The vertex function for the $\pi N \to \Delta$ transition is expressed as

$$F^{\dagger}_{\pi N\Delta} = -i\sqrt{6\pi^2}\sqrt{\frac{2\omega_\pi E_p}{M_N}} g_{\pi N\Delta}(p)(\mathbf{S}^\dagger \cdot \hat{\mathbf{p}}), \tag{30}$$

where p is the three momentum in the πN center of mass system and $\hat{\mathbf{p}}$ is its unit vector. $\mathbf{S}^\dagger$ is the spin transition operator from 1/2 to 3/2 and $g_{\pi N\Delta}$ is given by [18]

$$g_{\pi N\Delta}(p) = \frac{F_\Delta}{\sqrt{2(m_\pi + M_N)}} \frac{p}{m_\pi} \left(\frac{Q^2_\Delta}{Q^2_\Delta + p^2} \right)^2, \tag{31}$$

where F_Δ is the coupling constant and Q_Δ is the range parameter. The Δ self-energy $\Sigma^\Delta_{\pi N}$ is evaluated using the vertex function $F^{\dagger}_{\pi N\Delta}$. The parameters M^0_Δ, F_Δ, and Q_Δ were adjusted to fit the experimental P_{33} scattering amplitude [18].

The πN scattering t matrix in the D_{13} channel has the same form with the above P_{33} amplitude t_{P33} as follows:

$$t_{D13} = \frac{F_{\pi NN^*} F^{\dagger}_{\pi NN^*}}{\sqrt{s} - M^0_{N^*} - \Sigma^{N^*}_{\text{total}}}, \tag{32}$$

where $M^0_{N^*}$ denotes the bare mass of N^*. The vertex function for the $\pi N \to N^*$ transition is written as [19]

$$F^{\dagger}_{\pi NN^*} = -i(2\pi)^{3/2}\sqrt{\frac{2\omega_\pi E_p}{M_N}}\frac{f_{\pi NN^*}}{\sqrt{2(m_\pi + M_N)}}\left(\frac{p}{p_{\pi NN^*}}\right)^2 \times e^{-(p/p_{\pi NN^*})^2}(S^{(2)\dagger}\cdot Y_2(\hat{\mathbf{p}})), \tag{33}$$

where $f_{\pi NN^*}$ is the πNN^* coupling constant and $p_{\pi NN^*}$ is the πNN^* range parameter. $S^{(2)\dagger}$ is the second-rank spin transition operator from 1/2 to 3/2, which is defined by

$$S^{(2)\dagger} = \sqrt{\frac{2}{5}}[\mathbf{S}^{\dagger}\times\boldsymbol{\sigma}]^{(2)}. \tag{34}$$

The $N^*(1520)$ resonance can decay into both the πN and $\pi\pi N$ channels. The $\pi\pi N$ decay occurs through three dominant modes, i.e., $(\pi\Delta)_{s-wave}$, $(\pi\Delta)_{d-wave}$, and ρN. These branching fractions are known to be comparable. Thus the total N^* self-energy (Σ_{total}) is expressed as

$$\Sigma^{N^*}_{\text{total}} = \Sigma^{N^*}_{\pi N} + \Sigma^{s}_{\pi\Delta} + \Sigma^{d}_{\pi\Delta} + \Sigma_{\rho N}, \tag{35}$$

where $\Sigma^{N^*}_{\pi N}$, $\Sigma^{s}_{\pi\Delta}$, $\Sigma^{d}_{\pi\Delta}$, and $\Sigma_{\rho N}$ are due to the coupling to the πN, s-wave $\pi\Delta$, d-wave $\pi\Delta$, and ρN channels, respectively. $\Sigma^{N^*}_{\pi N}$ is evaluated from the vertex function $F^{\dagger}_{\pi NN^*}$ and the other components of the self-energy are obtained from the following vertex functions:

$$F^{s\dagger}_{\pi\Delta N^*}(p) = -i(2\pi)^{3/2}\sqrt{\frac{2\omega_\pi}{2(m_\pi + M_N)}}f^{s}_{\pi\Delta N^*} \times e^{-(p/p^{s}_{\pi\Delta N^*})^2}Y_{00}(\hat{\mathbf{p}}) \tag{36}$$

for the $N^* \to (\pi\Delta)_{s-wave}$,

$$F^{d\dagger}_{\pi\Delta N^*}(p) = -i(2\pi)^{3/2}\sqrt{\frac{2\omega_\pi}{2(m_\pi + M_N)}}f^{d}_{\pi\Delta N^*}\left(\frac{p}{p^{d}_{\pi\Delta N^*}}\right)^2 \times e^{-(p/p^{d}_{\pi\Delta N^*})^2}(S^{(2)\dagger}_{3/2}\cdot Y_2(\hat{\mathbf{p}})), \tag{37}$$

for the $N^* \to (\pi\Delta)_{d-wave}$, and

$$F^{\dagger}_{\rho NN^*} = (2\pi)^{3/2}\sqrt{\frac{2\omega_\rho E_p}{M_N}}f_{\rho NN^*}e^{-(p/p_{\rho NN^*})^2}(\mathbf{S}^{\dagger}\cdot\boldsymbol{\varepsilon}_\rho)Y_{00}(\hat{\mathbf{p}}), \tag{38}$$

for the $N^* \to \rho N$. Here $f^{s}_{\pi\Delta N^*}$, $f^{d}_{\pi\Delta N^*}$, and $f_{\rho NN^*}$ are the s-wave, d-wave $\pi\Delta N^*$, and ρNN^* coupling constants, respectively. $p^{s,d}_{\pi\Delta N^*}$ and $p_{\rho NN^*}$ are the $\pi\Delta N^*$ and ρNN^* range parameters. $S^{(2)\dagger}_{3/2}$ is the second-rank spin transition operator from 3/2 to 3/2 defined in Ref. [12]. $\Sigma^{s(d)}_{\pi\Delta}$ and $\Sigma_{\rho N}$ contain the effect of the decay process $\Delta \to \pi N$ or $\rho \to \pi\pi$ and their explicit forms are given in Ref. [12].

In this paper, we simply choose 400 MeV/c for the range parameters ($p_{\pi NN^*}, p^{s}_{\pi\Delta N^*}, p^{d}_{\pi\Delta N^*}, p_{\rho NN^*}$) which reproduces the nucleon size in quark models [19]. The coupling constants ($f_{\pi NN^*}, f^{s}_{\pi\Delta N^*}, f^{d}_{\pi\Delta N^*}, f_{\rho NN^*}$) and the bare mass ($M^0_{N^*}$) are adjusted to fit the N^* resonance energy, its width and the branching ratios at the resonance energy. We use 1520 MeV as the resonance energy and 120 MeV as the width, respectively. We take a fraction of 60% for the decay into πN, 8% into s-wave $\pi\Delta$, 12% into d-wave $\pi\Delta$, and 20% decay into the ρN channel, respectively [20], which are slightly different from the values used in the previous model [12,13]. We note that the parameters cannot be uniquely fixed due to the limited experimental information and their uncertainties. The parameter set used in this paper are given in Table I. The signs of the coupling constants are the same as those in Ref. [13]. With this parametrization, the πN D_{13} scattering amplitudes calculated agree with the data around the resonance energy but are deviated as the pion energy is away from it. The range parameters are necessary to be varied in order to get good agreement with the data over a wide range of the pion energies, but they are not uniquely determined in the present case and the fitted parameter sets include a very small range parameter which is hardly acceptable from a physical point of view. Furthermore, the

TABLE I. Parameter set for N^* used in this paper.

$f_{\pi NN^*}$	$f^{s}_{\pi\Delta N^*}$	$f^{d}_{\pi\Delta N^*}$	$f_{\rho NN^*}$	$M^0_{N^*}$(MeV)
1.147	0.398	1.435	0.942	1709.

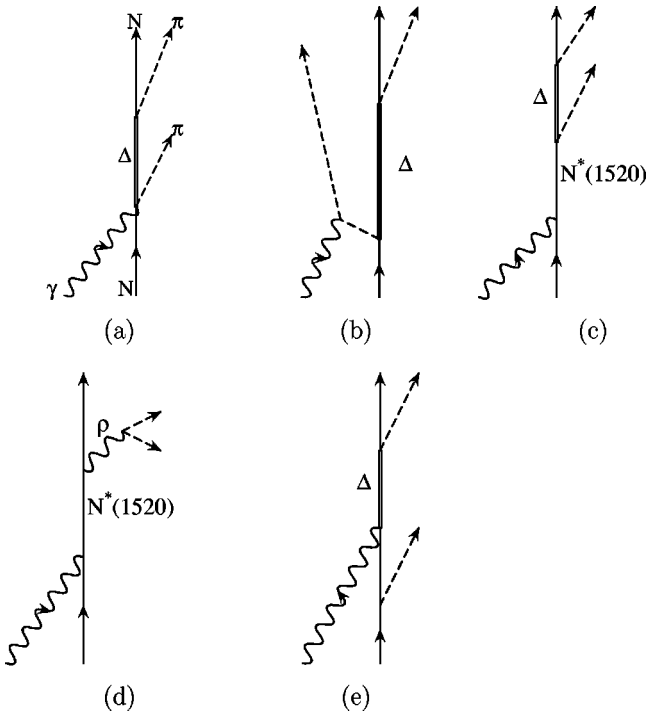

FIG. 5. Diagrams of resonant processes. (a) the Δ Kroll-Ruderman term ($T_{\Delta KR}$), (b) Δ pion-pole term ($T_{\Delta PP}$), (c) N^* excitation terms ($T^{s(d)}_{N^*\pi\Delta}$), (d) N^* excitation terms ($T_{N^*\rho N}$), and (e) the $\pi\Delta$ production term accompanied by nucleon exchange ($T_{\Delta nex}$).

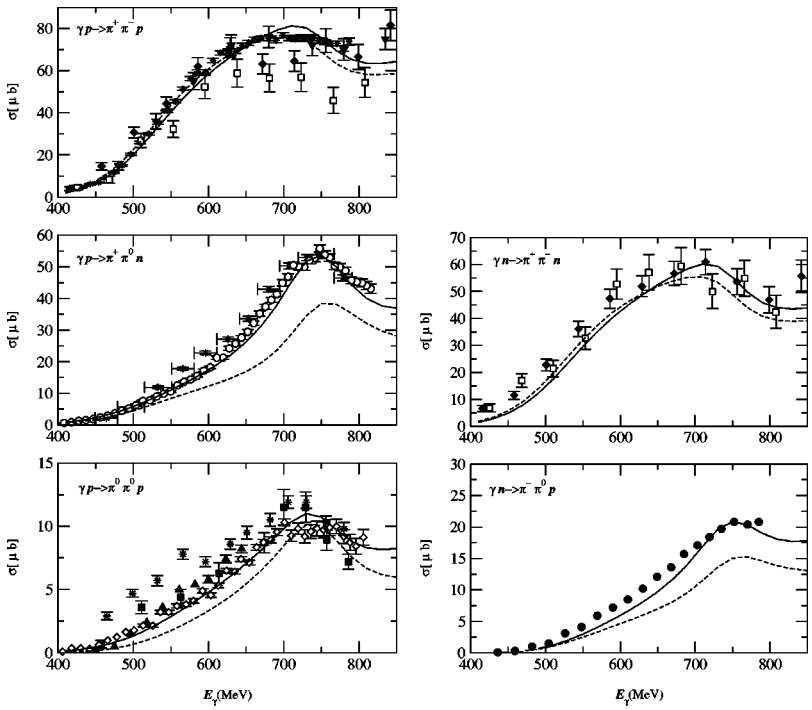

FIG. 6. Total cross sections of two-pion photoproduction on proton and neutron in various isospin channels. The solid and dashed lines correspond to the PS and PV calculations. Data are from Refs. [1](triangle down), [2](open square), [4](black diamond), [5](star), [6](open circle), [7](triangle up and black square), [8](open diamond), and [9](black circle). The data (black circle) of $\gamma n \to \pi^- \pi^0 p$ correspond to the cross section over the DAPHNE acceptance.

background πN interaction may be needed and thus one must go beyond the present framework of the isobar model. We think that the above description for N^* is sufficient for the present purpose, namely, to examine the difference between the PS and PV couplings.

Now we consider the resonant couplings by photon. The $\gamma N\Delta$ and γNN^* coupling constants can be determined by using the multipole amplitudes in the relevant channel for the $\gamma N \to \pi N$ reaction. The multipole amplitudes for the $\gamma N \to \pi N$ reaction have non-negligible background contributions and thus are generally expressed as the sum of the background and resonant terms, i.e.,

$$T^{\gamma N} = T_B^{\gamma N} + T_R^{\gamma N}. \tag{39}$$

Like the πN elastic scattering amplitudes, the resonant term $T_R^{\gamma N}$ is given by the isobar model as

$$T_\Delta^{\gamma N} = \frac{F_{\pi N\Delta} F^\dagger_{\gamma N\Delta}}{\sqrt{s} - M_\Delta^0 - \Sigma^\Delta_{\pi N}} \tag{40}$$

for the Δ resonance and

$$T_{N^*}^{\gamma N} = \frac{F_{\pi NN^*} F^\dagger_{\gamma NN^*}}{\sqrt{s} - M_{N^*}^0 - \Sigma^{N^*}_{\text{total}}} \tag{41}$$

for the N^* resonance.

The Δ resonance can contribute to both $M_{1+}(3/2)$ and $E_{1+}(3/2)$ multipole amplitudes. Since the magnitude of the $E_{1+}(3/2)$ multipole is small compared with $M_{1+}(3/2)$, the $E2$ $\gamma N\Delta$ coupling is neglected. The $\gamma N \to \Delta$ vertex function for the $M_{1+}(3/2)$ channel is written as

$$F^\dagger_{\gamma N\Delta} = -ig_{M_{1+}} \mathbf{S}^\dagger \cdot \mathbf{k} \times \boldsymbol{\epsilon}, \tag{42}$$

where $g_{M_{1+}}$ and $\boldsymbol{\epsilon}$ are the $M1$ $\gamma N\Delta$ coupling constant and photon polarization vector, respectively, and $\mathbf{k}$ denotes the initial photon momentum. We use $g_{M_{1+}} = 0.1991$ (in natural unit), which is obtained from the resonant coupling given by the Particle Data Group [20].

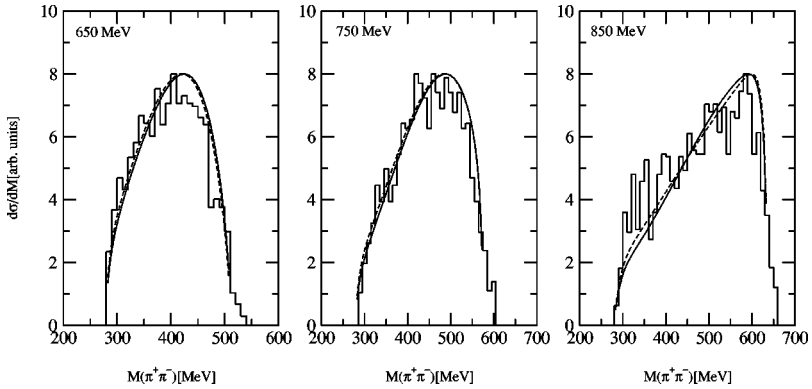

FIG. 7. Invariant mass spectra of $\pi\pi$ for $\gamma p \to \pi^+ \pi^- p$ at 650, 750, and 850 MeV. The solid and dashed lines correspond to the PS and PV calculations, respectively. Data are normalized appropriately and from Ref. [1].

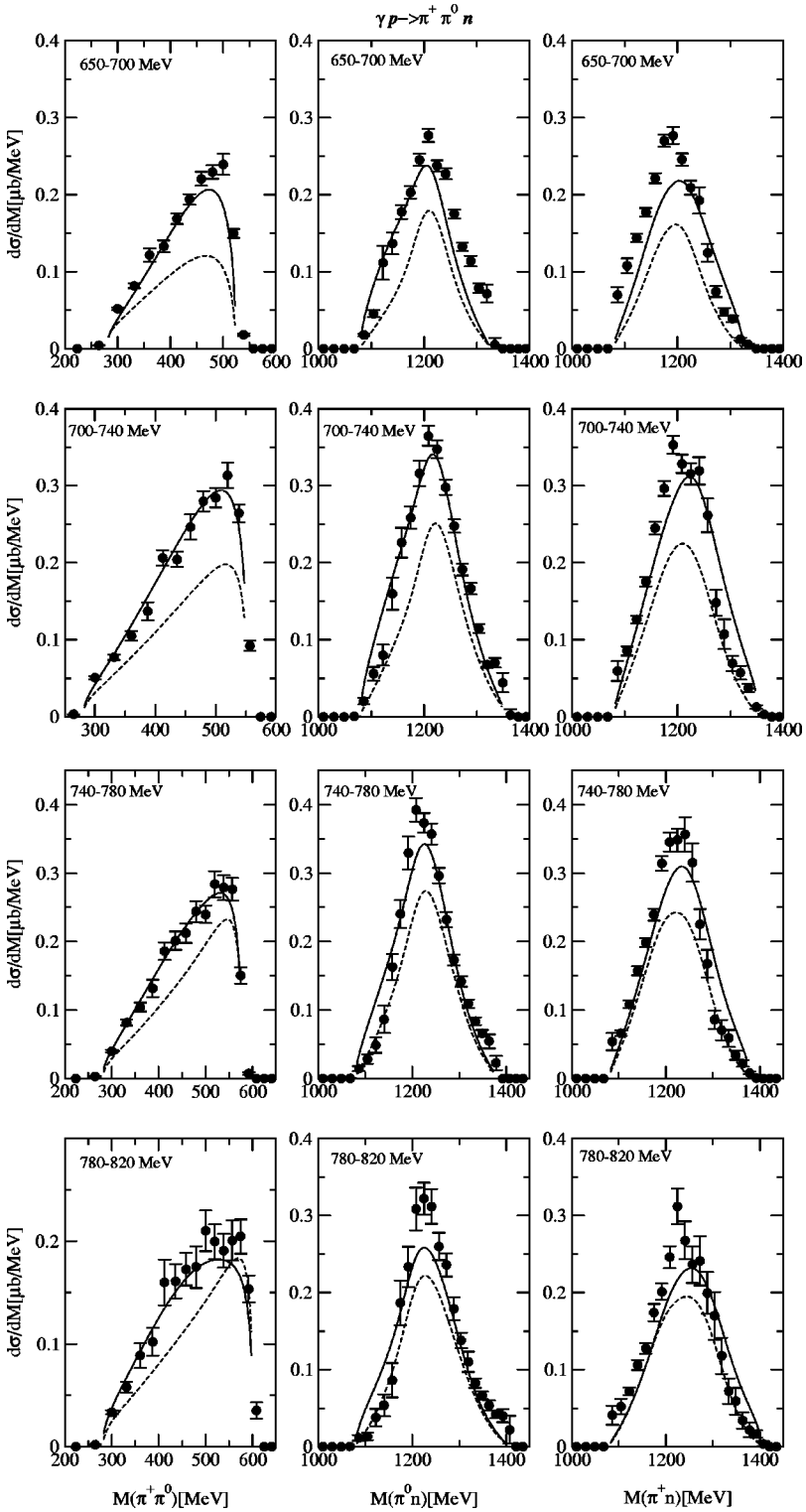

FIG. 8. Invariant mass spectra of $\pi^+\pi^0$, $\pi^0 n$, and $\pi^+ n$ for $\gamma p \to \pi^+\pi^0 n$ at four bins of incident photon energy. The solid and dashed lines correspond to the PS and PV calculations, respectively. Data are from Ref. [6].

For the N^* resonance, we use the helicity amplitudes instead of the electric and magnetic multipoles. The γNN^* vertex has two independent helicity couplings: the helicity 1/2 and 3/2 couplings. For the helicity 1/2 transition, $F^{\dagger}_{\gamma NN^*}$ is written as

$$F^{1/2\dagger}_{\gamma NN^*} = -ig_{1/2}(\mathbf{S}^{\dagger}\cdot\hat{\mathbf{k}})(\boldsymbol{\sigma}\cdot\hat{\mathbf{k}}\times\boldsymbol{\epsilon}), \tag{43}$$

where $g_{1/2}$ is the helicity 1/2 coupling constant and $\hat{\mathbf{k}}$ denotes the unit vector of the initial photon momentum. For the helicity 3/2 transition, $F^{\dagger}_{\gamma NN^*}$ is written as

$$F^{3/2\dagger}_{\gamma NN^*} = g_{3/2}\left\{(\mathbf{S}^{\dagger}\cdot\boldsymbol{\epsilon}) + \frac{i}{2}(\mathbf{S}^{\dagger}\cdot\hat{\mathbf{k}})(\boldsymbol{\sigma}\cdot\hat{\mathbf{k}}\times\boldsymbol{\epsilon})\right\}, \tag{44}$$

where $g_{3/2}$ is the helicity 3/2 coupling constant. For the pro-

ton target, the helicity 1/2 amplitude is small compared with the helicity 3/2 amplitude and so the helicity 1/2 coupling is neglected. For the neutron target, both couplings are taken into account. We use $g_{1/2}=0$ and $g_{3/2}=0.1612$ for the proton target and $g_{1/2}=-0.0496$ and $g_{3/2}=-0.135$ for the neutron target, respectively, which are obtained from the resonant couplings given by the Particle Data Group [20].

Generally, the $\gamma N\Delta$ and γNN^* coupling constants $(g_{M_{1+}},g_{1/2},g_{3/2})$ include both bare couplings to the resonances and vertex corrections due to the interference with the background processes and thus are complex and energy dependent in nature. One way to determine the coupling constants is to extract them from the experimental multipole amplitudes by assuming an appropriate nonresonant background term $T_B^{\gamma N}$. The other way is to use the resonance couplings given by the Particle Data Group [20] which correspond to the bare couplings. In most of previous models [11,10,14], real coupling constants obtained by the latter method have been used to calculate the cross sections for the two-pion photoproduction. Since the imaginary values are small for these resonances as predicted in the phenomenological calculations [16], we also employed the latter method for simplicity.

B. Resonant amplitude of $\gamma N\rightarrow\pi\pi N$

We use the same approach with the model of Ref. [12,13] for the resonance production processes and make a brief review about it in this section. The resonant T_R matrix for the two-pion photoproduction is expressed as

$$T_R=T_{\Delta KR}+T_{\Delta PP}+T^s_{N^*\pi\Delta}+T^d_{N^*\pi\Delta}+T_{N^*\rho N}+T_{\Delta nex}. \tag{45}$$

The resonant T_R matrix consists of six amplitudes: the Δ Kroll-Ruderman term ($T_{\Delta KR}$), Δ pion-pole term ($T_{\Delta PP}$), N^* excitation terms ($T^{s(d)}_{N^*\pi\Delta}$ and $T_{N^*\rho N}$) and the $\pi\Delta$ production term accompanied by nucleon exchange ($T_{\Delta nex}$). These diagrams are shown in Figs. 5(a)–5(e), respectively. The strength of these resonant processes depends strongly on the isospin channel [10,12]. The terms $T_{\Delta KR}$ and $T_{\Delta PP}$ dominate for the $\pi^+\pi^-$ production and becomes small due to the isospin factor for the $\pi^+\pi^0$ ($\pi^-\pi^0$) production and then are prohibited for the $\pi^0\pi^0$ production. Although the N^* excitation terms have only weak strength, they contribute to all isospin channel and their interference with the Δ Kroll-Ruderman term has significant effects to the cross section. The other processes arising from the requirement of the gauge invariance are neglected because they are known to be small.

The Δ Kroll-Ruderman term is written as

$$T_{\Delta\mathrm{KR}}=\frac{F_{\pi N\Delta}F^\dagger_{\Delta\mathrm{KR}}}{\sqrt{s}-\omega_\pi-E_\Delta-\Sigma_\Delta^{(\pi N)}(q,\sqrt{s})}, \tag{46}$$

where $\omega_\pi=\sqrt{m_\pi^2+q^2}$ and $E_\Delta=\sqrt{(M_\Delta^0)^2+q^2}$. $\Sigma_\Delta^{(\pi N)}(q,\sqrt{s})$ is the self-energy of Δ moving with the momentum q that arises from the coupling to the πN channel. Its expression is given in Ref. [19]. The $\gamma N\pi\Delta$ contact term operator $F^\dagger_{\Delta\mathrm{KR}}$ is obtained from the strong $\pi N\Delta$ vertex function so as to satisfy the gauge invariance, the detail of which is given in Ref. [12]. Instead of using the effective Lagrangian [10], we employ the vertex function with a form factor. The $N\rightarrow\pi\Delta$ transition operator is assumed to have the same form as the $\Delta\rightarrow\pi N$ vertex function. Since the range parameter $Q_\Delta(N\rightarrow\pi\Delta)$ is not necessarily the same as the parameter Q_Δ in Eq. (31) and thus is unknown, we treat it as a free parameter and vary it to fit the $\gamma p\rightarrow\pi^+\pi^-p$ cross section. The pion-pole term $T_{\Delta PP}$ is obtained by replacing $F^\dagger_{\Delta\mathrm{KR}}$ in Eq. (46) with the $\gamma N\pi\Delta$ pion-pole vertex function $F^\dagger_{\Delta\mathrm{PP}}$, whose detailed expression is given in Ref. [12].

The $\gamma N\rightarrow N^*\rightarrow\pi\pi N$ transition takes place the following two possible processes: $N^*\rightarrow\pi\Delta$ (s-wave or d-wave $\pi\Delta$ states) and $N^*\rightarrow\rho N$. They are described by $T^{s(d)}_{N^*\pi\Delta}$ and $T_{N^*\rho N}$, respectively. Using the isobar model mentioned in the preceding section, the T matrix elements of $T^{s(d)}_{N^*\pi\Delta}$ and $T_{N^*\rho N}$ are written as

$$T^{\mathrm{s(d)}}_{N^*\pi\Delta}=\frac{F_{\pi N\Delta}F^{s(d)\dagger}_{\pi\Delta N^*}F^\dagger_{\gamma NN^*}}{[\sqrt{s}-\omega_\pi-E_\Delta-\Sigma_\Delta^{(\pi N)}(q,\sqrt{s})](\sqrt{s}-M^0_{N^*}-\Sigma^{N^*}_{\mathrm{total}})}, \tag{47}$$

$$T_{N^*\rho N}=\frac{F_{\rho\pi\pi}F_{\rho NN^*}F^\dagger_{\gamma NN^*}}{2\omega_\rho[\sqrt{s}-\omega_\rho-E_{q_\rho}-\Sigma_{\rho\pi\pi}(q_\rho,\sqrt{s})](\sqrt{s}-M^0_{N^*}-\Sigma^{N^*}_{\mathrm{total}})}, \tag{48}$$

respectively. Here, q_ρ is the momentum of ρ meson and $\Sigma_{\rho\pi\pi}(q_\rho,\sqrt{s})$ is the self-energy of ρ meson moving with the momentum q_ρ. The ρ meson is described by the isobar model [see Eq. (27)].

The $\pi\Delta$ production term accompanied by nucleon exchange is written as

$$T_{\Delta nex}=\frac{F_{\pi N\Delta}F^\dagger_{\gamma N\Delta}F^\dagger_{\pi NN}}{[\sqrt{s}-\omega_\pi-E_\Delta-\Sigma_\Delta^{(\pi N)}(q,\sqrt{s})](E_k-\omega_\pi-E_{k+q})}, \tag{49}$$

where the πNN vertex function $F^\dagger_{\pi NN}$ is assumed to have a

usual nonrelativistic form. Unlike the other resonant processes, the intermediate particle, i.e., nucleon, is far off-shell. Since only the on-shell resonant $M_{1+}(3/2)$ multipole amplitude is known, some prescription is needed to include the off-shell effect in the above T matrix [Eq. (49)]. We take the modified pole approximation [21] where the angular part of $F^{\dagger}_{\gamma N\Delta}$ is evaluated at the center of mass system of γN and its magnitude is evaluated at the total energy of the final πN state. The contribution of $T_{\Delta nex}$ to the cross sections is expected to be small due to the off-shell effect. However, we include this amplitude in our calculations, since it becomes non-negligible for the $\gamma p \to \pi^0\pi^0 p$ reaction due to large coupling constants in $M_{1+}(3/2)$ channel.

IV. NUMERICAL RESULTS AND DISCUSSIONS

In this section, we present our numerical results of total cross sections, invariant mass spectra and helicity-dependent cross sections obtained by using the model introduced in the previous sections and compare them with the experimental data. In our model, the T matrix for the two-pion photoproduction is written as

$$T = T_{NR} + T_R, \tag{50}$$

where T_{NR} is the nonresonant T matrix given in Sec. II and T_R is the resonant T matrix [Eq. (45)] in Sec. III. For T_{NR}, we consider two kinds of models: PS and PV models with vector meson contributions. Correspondingly there are two kinds of full T matrices for Eq. (50) which are expressed as T_{PS} and T_{PV}, respectively. To demonstrate the difference of πNN couplings, we always compare the calculations by T_{PS} with those by T_{PV} which are shown in figures below.

In our model, there is a free parameter: the range parameter $Q_\Delta(N\to\pi\Delta)$ of the $N\to\pi\Delta$ vertex function appearing in the Δ Kroll-Ruderman term. At present we do not know how to determine it by using other reactions than the two-pion photoproduction. We use $Q_\Delta(N\to\pi\Delta)=430$ MeV/c determined so as to reproduce the $\gamma p\to\pi^+\pi^- p$ cross sections. Here the $N\to\pi\Delta$ vertex function is assumed to have the same form with the $\Delta\to\pi N$ vertex function used in this paper, since the Δ propagator used in Eq. (46) is calculated with the same $\Delta\to\pi N$ vertex function. In this sense, we think, it is not appropriate to use the monopole type of form factor employed by the authors of Refs. [10,14] in our approach. Although the value of $Q_\Delta(\Delta\to\pi N)$ is taken to be 358 MeV/c given by Betz and Lee [18], the value of $Q_\Delta(N\to\pi\Delta)$ does not need to be the same, since the form factors for $\Delta\to\pi N$ and $N\to\pi\Delta$ are functions depending on the relative momentum of πN and $\pi\Delta$ systems, respectively. At a given relative momentum, in fact, the square of the pion four-monentum evaluated in the πN center-of-mass system is larger than that in the $\pi\Delta$ center-of-mass system due to the mass difference between N and Δ.

First, we show the results of the total cross sections of five isospin channels, i.e., $\gamma p\to\pi^+\pi^- p$, $\gamma p\to\pi^+\pi^0 n$, $\gamma p\to\pi^0\pi^0 p$, $\gamma n\to\pi^+\pi^- n$, and $\gamma n\to\pi^-\pi^0 p$, in Fig. 6. Here the calculations with T_{PS} and T_{PV} are presented with the solid and dashed lines, respectively. We find that the PS calculations are in good agreement with the data in all channels and on the other hand the PV calculations underestimate the data except for $\pi^+\pi^-$ channels. The discrepancy between two calculations is clearly due to the difference of the nonresonant processes. Our results of the $\gamma p\to\pi^+\pi^0 n$ and $\gamma p\to\pi^0\pi^0 p$ reactions for the PV model are not consistent with those by the model of Nacher *et al.* [14], where the nonresonant amplitudes are constructed using the nonrelativistic PV πNN coupling. Their results are more close to the experimental data compared with our result for the PV model. We think that this inconsistency comes mainly from the way of the calculation of the diagram (e) in Fig. 5, where the nucleon in the intermediate state is far off-shell. We have evaluated this diagram with the modified pole approximation and on the other hand they adopted simply the $\gamma N\Delta$ vertex function without cutoff factor that has a linear dependence of the photon momentum. Consequently, the $\gamma N\Delta$ coupling becomes very large in the energy region of the $N^*(1520)$ resonance and leads to the large cross section.

Second, we calculated the invariant mass spectra of three isospin channels, i.e., $\gamma p\to\pi^+\pi^- p$, $\gamma p\to\pi^+\pi^0 n$, and $\gamma p\to\pi^0\pi^0 p$. The invariant mass spectra for the $\pi^+\pi^-$ system in the $\gamma p\to\pi^+\pi^- p$ channel are shown in Fig. 7. The calculations are performed with three photon energies, i.e., 650, 750, and 850 MeV. In this case, the values of the data are plotted arbitrarily and the calculations are normalized so as to fit the peak value of the experimental distributions. For the shape, two calculations (PS and PV calculations) are almost equivalent each other and are in good agreement with the data.

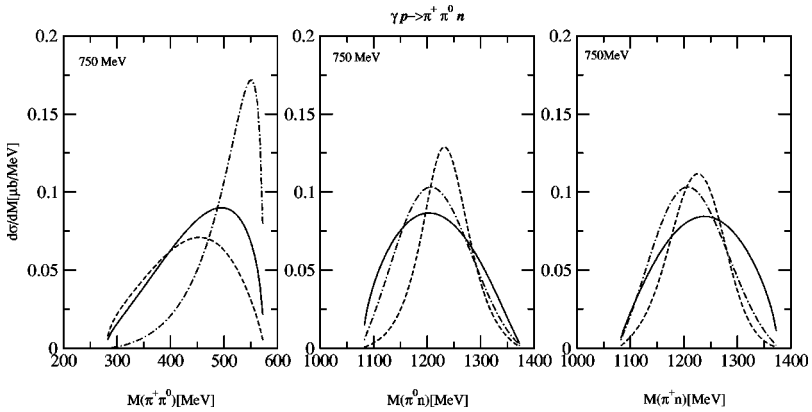

FIG. 9. Contributions of resonant processes in invariant mass spectra of $\pi^+\pi^0$, $\pi^0 n$, and $\pi^+ n$ systems for $\gamma p\to\pi^+\pi^0 n$ at 750 MeV. The dash-dotted and dashed lines are the calculations with $T_{N^*\rho N}$ and $T_{\Delta KR}+T_{\Delta PP}+T_{\Delta nex}+T^s_{N^*\pi\Delta}+T^d_{N^*\pi\Delta}$ (see text), respectively. The nonresonant PS calculation (solid line) is also plotted.

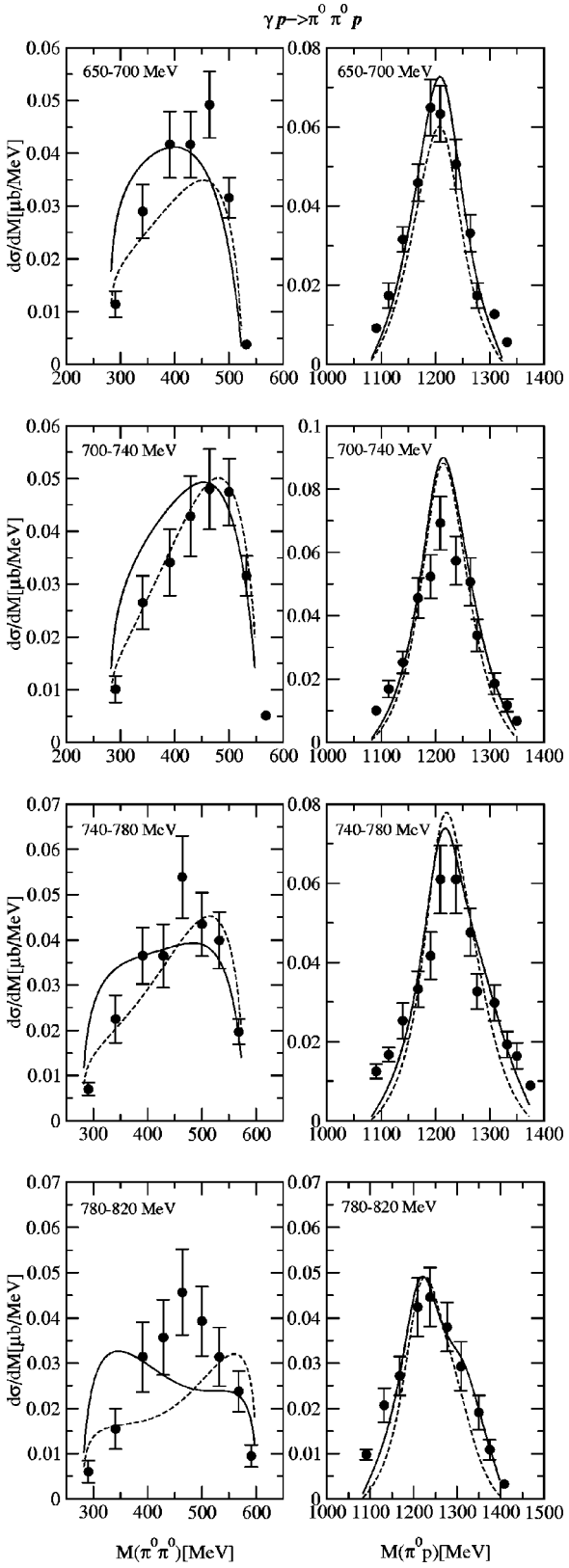

FIG. 10. Invariant mass spectra of $\pi^0\pi^0$ and $\pi^0 p$ for $\gamma p \rightarrow \pi^0\pi^0 p$ at four bins of incident photon energy. The solid and dashed lines correspond to the PS and PV calculations, respectively. Data are from Ref. [8].

For the $\gamma p \rightarrow \pi^+\pi^0 n$ channel, the invariant mass spectra for the $\pi^+\pi^0$, $\pi^0 n$ and $\pi^+ n$ systems are calculated at four bins of photon energies, i.e., 650–700 MeV, 700–740 MeV, 740–780 MeV, and 780–820 MeV and are shown with the data in Fig. 8. We find that the PS calculations agree well with all data but the PV calculations show some discrepancy about the shape of the $\pi^+\pi^0$ invariant mass spectra in addition to the magnitude. The $\pi^+\pi^0$ invariant mass spectra have a peak shifted to the higher $\pi\pi$ invariant mass and the peak position of the $\pi^0 n$ and $\pi^+ n$ invariant mass spectra corresponds to the mass of $\Delta(1232)$. In order to see which process makes such behavior, the contributions of some components of the resonant processes are shown in Fig. 9. Here the dash-dotted and dashed lines correspond to the calculations with $T_{N*\rho N}$ and $T_{\Delta KR}+T_{\Delta PP}+T_{\Delta nex}+T^s_{N*\pi\Delta}+T^d_{N*\pi\Delta}$, respectively. For reference, the nonresonant PS calculations (solid lines) are also plotted in figures. Clearly, the peak shift for the $\pi^+\pi^0$ invariant mass distribution is due to the contribution of $N^* \rightarrow \rho N$ process and the peak position of the $\pi^0 n$ and $\pi^+ n$ invariant mass distribution is directly related to the $\Delta(1232)$ production in the intermediate state.

For the $\gamma p \rightarrow \pi^0\pi^0 p$ channel, the invariant mass spectra for the $\pi^0\pi^0$ and $\pi^0 p$ systems are calculated at the same bins of photon energies with the $\gamma p \rightarrow \pi^+\pi^0 n$ channel. The results are shown with the data in Fig. 10. In this channel, the Δ Kroll-Ruderman term [Fig. 5(a)] and pion pole terms [Fig. 5(b)] do not contribute to the cross section and so the magnitude of the cross section is rather small compared with other channels. Furthermore the $I=J=1$ $\pi\pi$ system such as the ρ meson is not produced because of isospin conservation. Therefore, only the processes of $T_{\Delta nex}, T^s_{N*\pi\Delta}$, and $T^d_{N*\pi\Delta}$ among the resonant processes contribute to the cross section in our model. We note that the production of the $I=J=0$ $\pi\pi$ system such as the σ meson could take place in this channel. From the comparison with the data, one finds that both PS and PV calculations can almost reproduce the data of the $\pi^0 p$ invariant mass spectra, which has a peak at the $\Delta(1232)$ mass. For the $\pi^0\pi^0$ invariant mass spectra, there are some discrepancies, especially, between PS calculations and the data. The PV calculations are almost consistent with the data except for the bin of 780–820 MeV, where there are two bumps in the distribution. On the other hand, the PS calculations show broader distributions than the data, arising from the nonresonant processes as shown in Fig. 4. In our calculations, the final state interactions for $\pi^0\pi^0$ and $\pi^0 p$ are not taken into account. As pointed out in Ref. [22], the final state interaction for $\pi^0\pi^0$ is expected to be important because of strong correlation between two pions in $I=J=0$ channel and the influence of the σ meson. Such effect might be one of the possibilities to improve the PS model and so it will be worthwhile to further study this channel by taking into account such effect.

Finally the calculations of the helicity-dependent cross sections $\sigma_{3/2}$ and $\sigma_{1/2}$ are shown with the data in Fig. 11. Here we display the cross sections in three isospin channels: the $\gamma p \rightarrow \pi^+\pi^- p$ cross section with the three charged particles in the DAPHNE acceptances [23,24], the $\gamma p \rightarrow \pi^+\pi^0 n$ cross section with the π^+ in the DAPHNE accep-

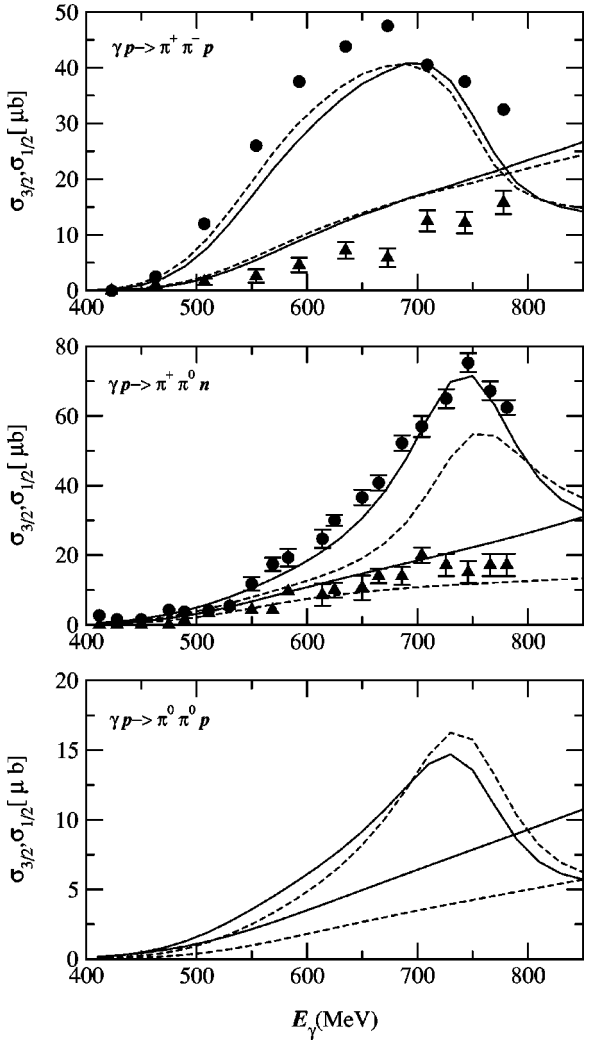

FIG. 11. Helicity-dependent cross sections $\sigma_{3/2}$ and $\sigma_{1/2}$ for $\gamma p \to \pi^+ \pi^- p$, $\gamma p \to \pi^+ \pi^0 n$, and $\gamma p \to \pi^0 \pi^0 p$. The solid and dashed lines correspond to PS and PV calculations, respectively. The upper two lines and black circles correspond to the cross section $\sigma_{3/2}$ and the other two lines and triangles correspond to the cross section $\sigma_{1/2}$ in each figure. In the above two figures of $\gamma p \to \pi^+ \pi^- p$ and $\gamma p \to \pi^+ \pi^0 n$, the cross sections over the DAPHNE acceptance are shown. Data are from Refs. [23,24].

tance [23,24] and the $\gamma p \to \pi^0 \pi^0 p$ cross section without kinematical limits for outgoing particles. The quantity $\sigma_{3/2}$ ($\sigma_{1/2}$) is defined as the cross section for the absorption of a polarized photon by a polarized target proton in the helicity 3/2 (1/2) channel. The solid and dashed lines denote the calculations with the PS model and PV model, respectively. It should be noted that the electromagnetic coupling of the $N^*(1520)$ to proton is known to be dominated by the helicity 3/2 state [20]. This is why the peak of the resonance is seen in the data for $\sigma_{3/2}$ but not for $\sigma_{1/2}$. Therefore, the cross section $\sigma_{1/2}$ is sensitive to the reaction mechanism not related to the $N^*(1520)$ resonance. For the $\gamma p \to \pi^+ \pi^- p$ reaction, one finds that the PS calculation is almost equivalent with the PV calculation like the total cross sections. Although the calculations agree qualitatively with the data, the cross section $\sigma_{3/2}$ is underestimated and the cross section $\sigma_{1/2}$ is overestimated. The detailed description of the reaction mechanism is still unsatisfactory for this channel and is needed to pursue what is missing in our model. For the $\gamma p \to \pi^+ \pi^0 n$ reaction, the PS model can almost explain two helicity-dependent cross sections simultaneously except for the cross section $\sigma_{1/2}$ around 750 MeV. On the other hand, the PV model underestimates the cross section $\sigma_{3/2}$ and also $\sigma_{1/2}$ slightly. In this model, nonresonant processes in the helicity 3/2 channel are not strong enough to explain the data. This result is not consistent with that obtained from the model by Nacher and Oset [23]. This is due to the same reason mentioned in the discussions of the total cross sections. For the $\gamma p \to \pi^0 \pi^0 p$ reaction, we observe that there is a large difference between the PS and PV models in the cross section $\sigma_{1/2}$. The experimental data, if they exist, could provide an important information on the reaction mechanism.

V. CONCLUDING REMARKS

Several theoretical studies on the two-pion photoproduction have been performed in the past but none of them have succeeded to reproduce the data in all isospin channels simultaneously. Particularly, unexpectedly large cross sections of the $\gamma p \to \pi^+ \pi^0 n$ and $\gamma n \to \pi^- \pi^0 p$ reactions were found not to be explained with the usual reaction mechanism and thus the presence of a new reaction mechanism in these channels is suggested. Ochi, Hirata, and Takaki [12] introduced the ρ Kroll-Ruderman term, which influences only on the above isospin channels, as a new reaction mechanism. However, a soft $\rho\pi\pi$ form factor was needed to reproduce the large cross sections and the isobar model with such a form factor failed to explain the $\pi\pi$ scattering at low energies. Thus, the ρ Kroll-Ruderman term was inferred to represent the effect of the background process followed by the production of the $I=J=1$ $\pi\pi$ system rather than the ρ meson itself.

In this paper, we have discussed the effect of the nonresonant processes arising from the PS and PV πNN couplings in the two-pion photoproduction in order to pursue an alternative reaction mechanism. The nonresonant amplitudes can be obtained by attaching an external photon line to the diagram of $N \to \pi\pi N$ calculated with the two πNN couplings. In order that the model with the PS πNN coupling is equivalent to the model with the PV πNN coupling in the strong interaction process $N \to \pi\pi N$, the effective contact interaction [Eq. (3)] is added to the former model. Using these models, we examined the effect of the two couplings on various isospin channels numerically. For the $\gamma p \to \pi^+ \pi^0 n$ and $\gamma n \to \pi^- \pi^0 p$ reactions, we found that the cross sections calculated with the PS model were larger than those with the PV model and their magnitude was almost consistent with the ρ Kroll-Ruderman used in Ref. [12]. Consequently, the nonresonant process described by the PS πNN coupling can be regarded as a candidate for the new reaction mechanism in place of the ρ Kroll-Ruderman term.

The importance of the PS πNN coupling in the two-pion photoproduction has not been so far noticed. In fact the nonresonant process has been always described by the PV πNN coupling and has been found to have only a minor contribu-

tion to the two-pion photoproduction. The PV πNN coupling is more favored than the PS πNN coupling for the $\gamma N \rightarrow \pi N$ reaction and the πN scattering at low energies. Therefore, the PV coupling has been also used for the $\gamma N \rightarrow \pi\pi N$ reaction as a matter of course. Recently, Drechsel *et al.* [16] pointed out in the study of the $\gamma N \rightarrow \pi N$ reaction that the PS coupling was needed to describe the data with the increase of the incident photon energy. This implies that the PS coupling is preferable to the PV coupling at larger off-shell nucleon momenta. Accordingly the PS coupling is expected to be important for the two-pion photoproduction, since the far off-shell nucleon is involved in the intermediate state.

In order to demonstrate the importance of the PS coupling and compare our theory with the data, we constructed two types of models (PS and PV models) by adding the vector meson contributions for the nonresonant processes (Fig. 2) as well as the $\Delta(1232)$ and $N^*(1520)$ contributions for the resonant processes (Fig. 5) to the nonresonant contributions coming from the πNN couplings (Fig. 1). Using these models, we calculated the total cross sections, invariant mass spectra and helicity-dependent cross sections for various isospin channels. Generally, these observables are successfully described by the PS model compared with the PV model except some details. Particularly the calculations of total cross sections and invariant mass spectra for the $\gamma p \rightarrow \pi^+\pi^0 n$ and $\gamma n \rightarrow \pi^-\pi^0 p$ channels by the PS model are in good agreement with the data and on the other hand those by the PV model are largely underestimated. There are some discrepancies between the calculations with the PS model and the data in the invariant mass spectra for the $\gamma p \rightarrow \pi^0\pi^0 p$ channel. Because the magnitude of the cross section in this channel is very small, the higher order processes might emerge in the detailed structure. Therefore, we think, it may be necessary to investigate the mechanism originating with the σ meson and the final state interaction which are not taken into account in our model. Although there are still unsatisfactory points, we conclude that the PS coupling certainly plays an important role in the two-pion photoproduction, especially, the $\gamma p \rightarrow \pi^+\pi^0 n$ and $\gamma n \rightarrow \pi^-\pi^0 p$ channels.

Now we would like to make some remarks about our model. First, the difference between the PS and PV couplings prominently appears in the neutral pion productions such as $\gamma p \rightarrow \pi^0 p$ and $\gamma p \rightarrow \pi^+\pi^0 n$ reactions. This is understood from the fact that it stems from the anomalous magnetic moment term in the γNN coupling [Eq. (4)] [25]. In fact the difference disappears if F_2 is set to zero. In our model, F_2 is taken to be the on-shell value. It would be interesting to find out the influence of the off-shell effects in the γNN vertex for the two-pion photoproduction and furthermore to know how the PS coupling at high photon energies is connected to the PV coupling at low energies in terms of the off-shellness of the intermediate nucleon. We note that the off-shell structure of the γNN vertex appears as the modification of the anomalous magnetic moment term [26].

Second, the resonant processes in the present model have been treated in a naive way. The strong coupling constants for the $N^*(1520)$ resonance are determined from its total width and the branching ratios given in Particle Data Group [20] and their form factor ranges are assumed to be consistent with the nucleon size in quark models. The electromagnetic couplings of the $N^*(1520)$ to nucleon are taken from the PDG and their values are real number. In order to investigate the role of the resonance in detail, the theory must be refined so as to describe three reactions, i.e., $\pi N \rightarrow \pi N$, $\gamma N \rightarrow \pi N$, and $\gamma N \rightarrow \pi\pi N$ simultaneously. For instance, the effective coupling constant of $\gamma NN^*(1520)$ becomes complex due to the interference with the background process, although its effect is not expected to be large because of the small imaginary number [16].

Finally, we have not included the $\Delta(1700)$ resonant process in our model. Nacher *et al.* [14] have pointed out that the $\Delta(1700)$ resonance has a significant contribution on the $\gamma N \rightarrow \pi\pi N$ reaction cross section due to the strong interference between the $\Delta(1700)$ resonant process and the Δ Kroll-Ruderman process although the contribution of only the $\Delta(1700)$ resonant process is almost negligible. They used the real $\gamma N\Delta(1700)$ coupling constant given in PDG like the $N^*(1520)$ resonance in our model. However, it was predicted in the phenomenological analysis of the $\gamma N \rightarrow \pi N$ reaction [16] that its imaginary part was comparable to its real part, which is quite different from the case of the $\gamma NN^*(1520)$ coupling. This complex coupling constant, if used, should largely influence the results of Ref. [14] about the interference effect. Further investigation is needed to draw a definite conclusion on the $\Delta(1700)$ resonant process.

ACKNOWLEDGMENTS

We would like to thank V. Metag for providing us the experimental data of the $\gamma p \rightarrow \pi^+\pi^0 n$ reaction.

[1] Aachen-Berlin-Bonn-Hamburg-Heidelberg-München Collaboration, Phys. Rev. **175**, 1669 (1968).
[2] A. Piazza *et al.*, Nuovo Cimento **3**, 403 (1970).
[3] G. Gialanella *et al.*, Nuovo Cimento A **63**, 892 (1969).
[4] F. Carbonara *et al.*, Nuovo Cimento A **36**, 219 (1976).
[5] A. Braghieri *et al.*, Phys. Lett. B **363**, 46 (1995).
[6] W. Langgärtner *et al.*, Phys. Rev. Lett. **87**, 052001 (2001).
[7] F. Härter *et al.*, Phys. Lett. B **401**, 229 (1997).
[8] M. Wolf *et al.*, Eur. Phys. J. A **9**, 5 (2000).
[9] A. Zabrodin *et al.*, Phys. Rev. C **55**, R1 (1997).
[10] J.A.G. Tejedor and E. Oset, Nucl. Phys. **A571**, 667 (1994); **A600**, 413 (1997).
[11] L. Y. Murphy and J. M. Laget, Report No. DAPNIA-SPHN-95-42.
[12] K. Ochi, M. Hirata, and T. Takaki, Phys. Rev. C **56**, 1472 (1997).

[13] M. Hirata, K. Ochi, and T. Takaki, Prog. Theor. Phys. **100**, 681 (1998).
[14] J.C. Nacher, E. Oset, M.J. Vicente Vacas, and L. Roca, Nucl. Phys. **A695**, 295 (2001).
[15] E. Oset, H. Toki, and W. Weise, Phys. Rep. **83**, 281 (1982).
[16] D. Drechsel, O. Hanstein, S.S. Kamalov, and L. Tiator, Nucl. Phys. **A645**, 145 (1999).
[17] I. Blomqvist and J.M. Laget, Nucl. Phys. **A280**, 405 (1977).
[18] M. Betz and T.-S.H. Lee, Phys. Rev. C **23**, 375 (1981).
[19] M. Arima, K. Masutani, and R. Seki, Phys. Rev. C **51**, 285 (1995).
[20] Particle Data Group, L. Montanet *et al.*, Phys. Rev. D **50**, 1173 (1994).
[21] E. Ferrari and F. Selleri, Nuovo Cimento **21**, 1028 (1961).
[22] E. Oset, L. Roca, M.J. Vicente Vacas, and J.C. Nacher, nucl-th/0112033.
[23] J.C. Nacher and E. Oset, Nucl. Phys. **A697**, 372 (2002).
[24] M. Lang for the GDH-and A2-Collaboration, in *Proceedings of GDH2000 Mainz, 2000*, edited by Drechsel and Tiator (World Scientific, Singapore, 2001).
[25] N. Katagiri and T. Takaki (unpublished).
[26] S. Kondratyuk, G. Martinus, and O. Scholten, Phys. Lett. B **418**, 20 (1998).